Available online at www.sciencedirect.com
SCIENCE DIRECT®
PERGAMON
International Journal of Heat and Mass Transfer 46 (2003) 4535–4551
International Journal of HEAT and MASS TRANSFER
www.elsevier.com/locate/ijhmt

Heat transfer in turbulent separated flows in the presence of high free-stream turbulence

V.I. Terekhov *, N.I. Yarygina [1], R.F. Zhdanov [2]

Kutateladze Institute of Thermophysics, Siberian Branch of Russian Academy of Sciences, 1 Acad. Lavrent'ev Avenue, Novosibirsk 630090, Russia

Abstract

Hydrodynamic features of the gas flows past a rib and past a downward step in characteristic separation-flow regions, and distributions of pressures, temperatures, and heat-transfer coefficients behind the obstacles in such flows were experimentally studied. A comparative analysis of the intensifying action of ribs and steps on convective heat transfer is given. We also examined the effect of enhanced external turbulence on thermal and dynamic characteristics of the separated flows. An increased level of free-stream turbulence suppresses the flow separation. The high free-stream turbulent intensifying effect turned out to be more pronounced for the flow past a downward step.

1. Introduction

Despite the substantial progress in experimental and numerical studies of turbulent flows with separation induced by various surface features, many details of heat-transfer processes in such flows still remain poorly understood in a broad range of free-stream parameters, which makes the extension of already gained data to separation flows of other geometric configurations rather difficult. The lack of necessary information is especially pressing if one considers the effect of flow prehistory, including high level of free-stream turbulence. First of all, here the problem of compiling reliable databases for such flows arises; such databases are necessary for revealing fundamental heat-transfer and dynamics regularities, and also for verification of new prediction algorithms and models for such flows.

The flow past a downward step is known to be a simplest example of flow with separation. The flow past a rib is more complicated since it displays an additional separation in the upstream region of the obstacle. A comparative study of the two cases enables gaining more information on heat transfer in separated flows and allows one to estimate the possibility of heat-transfer intensification or suppression by modifying the shape of obstacles or by introducing artificial perturbations into the approaching flow.

There are quite a number of reported studies for the flow past a downward step (see, for instance, the review in [1]). Many studies of the separation flow past a downward step were aimed at revealing its hydrodynamics (see [2,3]); heat-transfer problems for this flow were addressed more scarcely (see, for instance, [4]). It should be noted that the overwhelming majority of reported studies, although treating the matter in sufficient detail, represents in fact only particular problems. Among available literature sources, several papers report combined studies of flow dynamics and heat transfer in separation flows [5–7]; attempts have been made to generalize dynamics and heat-transfer data for the flow past a downward step and/or to reveal characteristic structural parameters of the flow (see, for instance, [8]). Of great interest here are studies in which broad ranges of geometric parameters (such as channel width [9] or step height [10]) were explored, and the effect of these parameters on characteristics of separated flows was considered. For instance, it was found

* Corresponding author. Tel.: +7-3832-341-736; fax: +7-3832-343-480.
E-mail addresses: terekhov@itp.nsc.ru (V.I. Terekhov), yarygina@itp.nsc.ru (N.I. Yarygina), zhdanov@itp.nsc.ru (R.F. Zhdanov).
[1] Tel.: +7-3832-391-336.
[2] Tel.: +7-3832-391-335.

0017-9310/$ - see front matter © 2003 Elsevier Ltd. All rights reserved.
doi:10.1016/S0017-9310(03)00291-6

Nomenclature

c_p	heat capacities of air (J/kg K)
C_p	pressure coefficient, $(P-P_0)/(\rho U_0^2/2)$
$\overline{C}_p$	specific pressure coefficient, $(C_p - C_{p\min})/(1-C_{p\min})$
H	height of rib or step (m)
Nu_H, Nu_x	Nusselt number, $\alpha H/\lambda$, $\alpha x/\lambda$
P	static pressure (N/m^2)
Pr	Prandtl number, $\mu c_p/\lambda$
Re_x, Re_S	Reynolds number, $U_0 x/\nu$, $U_0 S/\nu$
S	channel height (m)
St	Stanton number, $\alpha/(\rho U c_p)$
U	velocity (m/s)
q_w	local wall heat flux (W/m^2)
T, t	temperature (K)
Tu	free-stream turbulence intensity, $\sqrt{(\langle u^2\rangle + \langle v^2\rangle + \langle w^2\rangle)/3}/U$
x	streamwise coordinate (m)
y	vertical coordinate (m)
$\langle u^2\rangle$, $\langle v^2\rangle$, $\langle w^2\rangle$	root-mean-square velocity fluctuations (m^2/s^2)

Greek symbols

α	heat-transfer coefficient (W/(m^2 K))
β	step angle (grade)
δ	boundary-layer thickness (m)
η	specific vertical coordinate, $yU_0\sqrt{St}/\nu$
λ	thermal conductivity (W/(m K))
ϕ	specific temperature, $(T-T_w)/((T_0-T_w)\sqrt{St})$
μ	dynamic viscosity ((N s)/m^2)
ν	kinematic viscosity (m^2/s)
θ	dimensionless temperature, $(T-T_w)/(T_0-T_w)$
ρ	density (kg/m^3)

Subscripts

0	free-stream parameter in front of obstacle
max	maximum value
min	minimum value
R	parameter of reattachment region
Tu	turbulent parameter
**	integral parameter
w	wall parameter

possible to exert a profound influence on the heat-transfer maximum by changing the inclination angle of the step face [11].

The separation induced by a cross-flow plate (rib) was treated less extensively than the flow past a downward step (see, for instance, [12]). This is especially true in regard to heat transfer [13]. Although some works are available which analyze general physics of the separation phenomenon by comparing the flow past a downward step and the flow past a rib [14], no comparative data for ribs and downward steps were reported which would make it possible to perform an adequate (under identical flow conditions) comparison of the two types of obstacles. Such an analysis would be useful in studying characteristics of separated flows and their hydrodynamic features and, hence, in controlling flow separation and developing heat-transfer intensification methods.

Studies of characteristics of separation flows under complex external conditions, including high level of free-stream turbulence, are of considerable fundamental and practical significance. Gas and liquid flows in many technical apparatus are turbulent. For instance, the turbulence level in combustion chambers of gas turbine engines is normally in excess of 15%. If the separated flow develops under conditions of high free-stream turbulence, a question arises about the interaction between the separated flow and the high-turbulence main-stream flow. Up to date, simulations of turbulent heat transfer with due regard for dynamic parameters in the flow separation region still remain a problem difficult to solve. Involvement of an outside factor such as high level of free-stream turbulence further complicates the problem.

The papers in which the effect of turbulence on dynamic and, especially, thermal characteristics of rib- and step-induced separations was addressed are few in number. Moreover, the data gained in these works are rather contradictory even for a downward step, the most frequently addressed geometry. For instance, the authors of [15] argued that changes in the free-stream turbulence level in the range $Tu_0 = 1$–18% induce no substantial changes in the structure of the separated flow past a downward step and in the streamwise length of its characteristic regions. On the contrary, the authors of [16,17] found that, in their experiments, the length of the recirculation-flow region substantially depended on the level of free-stream turbulence. For instance, with increase in the turbulence level of the approaching flow from $Tu_0 = 1.6\%$ to 16% [17], the length of the recirculation zone was found to decrease by more than a factor of 1.6, although the rate of heat transfer at the flow-reattachment point showed no substantial dependence on this parameter. On the contrary, the authors of [13] observed a 30% increase in the maximum heat-transfer coefficient behind a cross-flow obstacle under the action of high free-stream turbulence.

All the aforesaid necessitates widening of the experiment and using it as the main means for gaining direct information about turbulent separation flows under complex external conditions and collecting data necessary for further development of prediction tools. Only extensive experimental information on flow dynamics and heat transfer will make it possible to adequately take into account the actual thermal phenomena in separation flows. Additional information about the structure of separation flows, regularities of transfer processes in them, and the inter-relation between hydrodynamic and thermal parameters, along with data on the effect of enhanced free-stream turbulence on these parameters, will help engineers to solve many problems concerning the control of such flows and choice of best design solutions. The present work, in which various experimental techniques were used, reports a set of experimental data on dynamics and heat transfer of separated flows past a rib and past a downward step under conditions of enhanced free-stream turbulence.

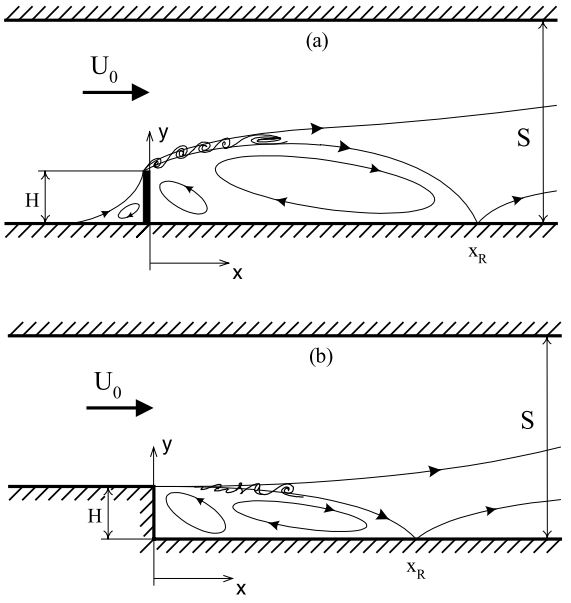

Fig. 1. Flow configuration behind a rib (a) and a downward step (b).

2. Experimental equipment and parameters

The experiments were carried out in a wind-tunnel facility with a 600-mm long rectangular channel. The channel had a 200×200 mm^2 cross-section. The flow velocity over obstacles was $U_0 = 20$ m/s, which corresponded to the Reynolds number Re_S, calculated by the channel height, of $\approx3\times10^5$. Either 3-mm thick ribs of various heights ($H = 3$, 6, 10, 20, and 30 mm) or a 60-mm high aerodynamic panel forming a downward step were mounted on the experimental model, a flat plate made of textolite. The model was 500-mm long, 200-mm wide, and 20-mm thick (Fig. 1). Required heights of downward steps ($H = 6$, 10, 20, or 30 mm) were obtained by vertical displacement of the lower plate, leaving the cross-sectional area of the inlet to the channel unchanged. In this manner, identical external conditions were ensured for studying separations behind downward steps of various heights under various levels of free-stream turbulence. In the experiments with inclined steps, the inclination angle of the step face (Fig. 2) was a varied parameter: $\beta = 90°$, 45°, 30°, 20°, and 15°; the step height in these experiments was either $H = 10$ or 20 mm.

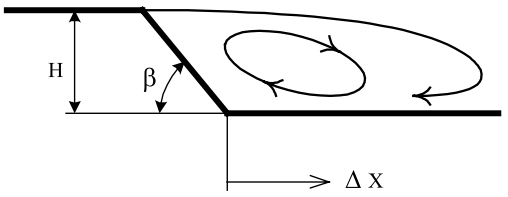

Fig. 2. The scheme of flow behind the backward-facing inclined step.

To turbulize the flow, two types of passive turbulence generators were used, one of the "perforated-plate" type and the other being a flag generator. The perforated plate had 81 holes 20 mm in diameter; the perforation degree was about 64%. The plate was installed in the nozzle of the wind-tunnel facility, upstream of its working section, at a distance of 330 mm from the obstacle (either rib or step). The flag generator was a perforated plate, identical to that described above, with flags–bands disposed at the nodes of the turbulizing grid. The turbulence level in the flow core at the obstacle plane (without the model) was 5% in the case of the turbulence generator of the first type (Fig. 3) and 13.4% in the case of the turbulence generator of the second type. The natural free-stream turbulence level of the wind-tunnel facility was 1.2%.

The heat-transfer tests were carried out in the regime $q_w = \text{const}$, using an ohmic heater prepared from a thin (10-μm thick) foil. The profiles of wall temperature along the centerline of the model were measured with the help of Chromel–Copel thermocouples installed equidistantly along this line with a 10-mm step. The heat leakages due to thermal conductivity in the model were calculated from the temperature difference across it. To measure the temperature difference, two thermocouples were additionally used, installed at the bottom of the model. To examine the dynamic losses, we measured the wall static pressure behind each of the obstacles. In these

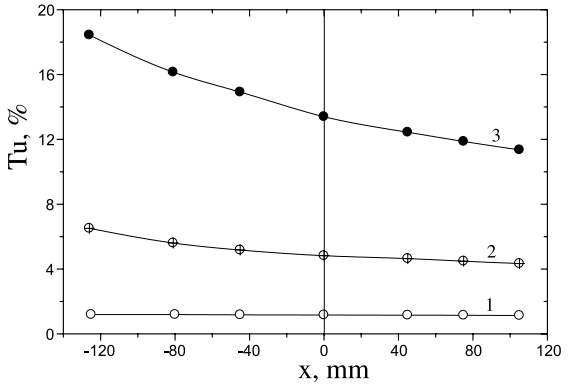

Fig. 3. Longitudinal velocity pulsation of free stream: (1) without turbulizator; (2) with "perforated" turbulizator; (3) with "flag" generator.

tests, a working section geometrically identical to the thermal one was used, which permitted pressure tapping through 0.3-mm diameter holes. The temperature profiles in the separation region were measured with the help of a 0.2-mm diameter thermocouple mounted on a special holder shaped so that to minimally disturb the flow. Additionally, thermographic visualization was performed to reveal the distribution of surface temperature. The graphite-epoxy coating on the surface of the model was a material with high electric conductivity; with this coating, a uniform heat flux from the model to the flow was ensured. The temperature field was digitized using 15 Chromel–Copel thermocouples embedded into the wall under the conducting layer and two additional thermocouples installed at the bottom of the model. The oil-film technique was employed to visualize the separation flows in the near-surface region.

Consider the behavior of major gas dynamic parameters at the flow separation point. Fig. 4 shows the flow-velocity profile and the profile of pulsating velocity over the plate in the cross-section where obstacles were subsequently installed, both under conditions of natural and enhanced free-stream turbulence. The velocity profiles (Fig. 4a) seem to be quite satisfactory, with some spatial non-uniformity displayed by the boundary layer only in the case of the flow turbulized by the flag turbulence generator. An insignificant compression of the flow due to model geometry somewhat decreased the turbulence level over the plate (Fig. 4b). The velocity profiles over the aerodynamic panel measured in the range of free-stream velocity $U_0 = 10$–30 m/s reveal a better filling of the boundary-layer velocity profile in the case of lower flow velocities at the inlet of the working section (Fig. 5). The data of Fig. 5 show that the boundary layer at the separation point was turbulent.

In line with the results of [18], the present heat-transfer tests for non-separated flows have shown the effect of enhanced free-stream turbulence on the rate of convective heat transfer at the symmetry axis of the plate to be insignificant (Fig. 6). The turbulence generator of the "perforated-plate" type caused a maximum increase in the Stanton number smaller than 4% of the similar effect observed under low-turbulence conditions. With the flag generator, the increase in the Stanton number amounted to about 15%.

3. Experimental data and their analysis

3.1. Dynamics of the separation flow. Effect due to high level of free-stream turbulence

Oil visualization of the surface behind obstacles allows one to estimate dimensions of characteristic zones of separation flows and reveal their formation pattern. The flow stalled from an obstacle hits the surface,

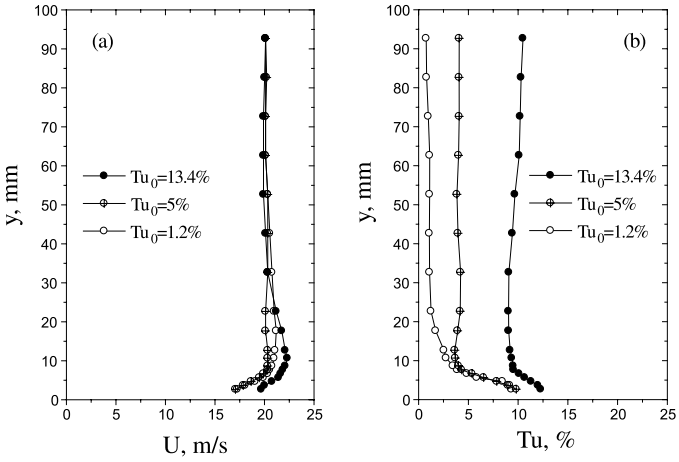

Fig. 4. Mean velocity (a) and turbulence intensity (b) profiles over the experimental plate before an obstacle.

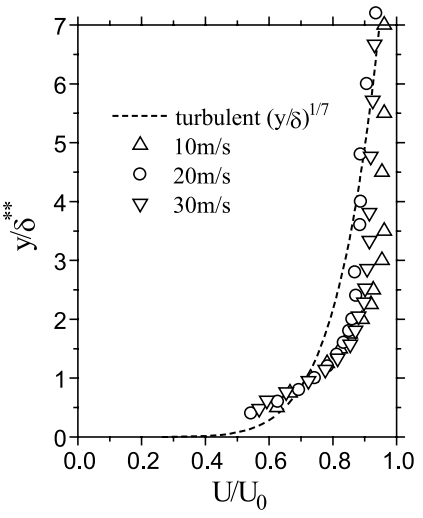

Fig. 5. Mean velocity profiles over a step for varying at low external turbulence ($\delta^{**} = 2$–2.5 mm).

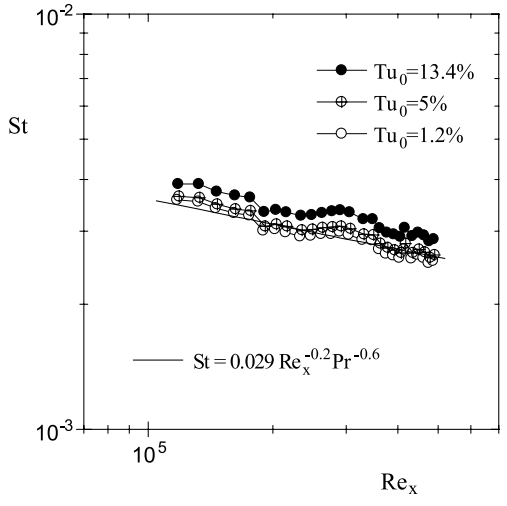

Fig. 6. Stanton number along a plate at three free-stream turbulence levels.

forming a flow-reattachment region (continuous white line in Figs. 7 and 8), and, subsequently, spreads over the surface both in the upstream and downstream directions. Under natural conditions, the time-mean position of the flow-reattachment point behind the 20-mm high rib on the symmetry plane of the plate (Fig. 7a) was $x_R/H \approx 16.5$. The reverse flow, approaching the obstacle after its reattachment to the surface, departs from the surface at a point remote from the rib approximately by two calibers, thus making the streamwise length of the main-recirculation vortex shorter, amounting only to 88% of the total length of the recirculation bubble. The authors of [12] reported a similar length for the main-recirculation vortex behind an obstacle with $H = 22$ mm. The oil visualization reveals intense, large-scale corner vortex structures in the secondary zone; these structures are normal to the surface (Fig. 7a). A change in the rib height causes no qualitative changes in the flow pattern. Meanwhile, the time-mean position of the flow-reattachment point behind the 10-mm high rib on the centerline of the plate (without artificial turbulization of the free flow) is $x_R/H = 18.5$ (Fig. 7c). Under identical external conditions, a decrease in the rib height gives rise to more pronounced bending of the reattachment curve and some elongation of the separation region in the streamwise direction (by about two calibers).

The high free-stream turbulence induces considerable changes into the flow pattern behind the same ribs, simultaneously not violating the symmetry of the flow. Under the action of the heavy turbulization of the free flow, the two large-scale vortices turn out to be shifted towards the rib and towards the corners, and they become smaller in size. The flow-reattachment point on the symmetry axis also gets shifted to $x_R/H \approx 13$ behind the 20-mm high rib (Fig. 7b) and to $x_R/H \approx 15$ behind the 10-mm high rib (Fig. 7d), and the time-mean flow-reattachment curve straightens in the transverse direction, in line with the observations reported in [19,20]. The main reason for the shrinkage of the separation zone with increasing level of free-stream turbulence is thickening of the mixing layer, which results in more rapid reattachment of the stalled flow and increased turbulent viscosity. The rectification of the flow-reattachment curve can be explained by more intense effect due to the three-dimensional structures developing in the mixing layer; these structures ensure communication between the near-rib region and the region immediately adjacent to the sidewalls.

A comparison between the visualization data obtained under identical natural conditions behind a rib (Fig. 7a and b) and behind a downward step (Fig. 8a and b) clearly demonstrate the difference in the reattachment pattern of the detached flows, in the development pattern of the reverse flow and, especially, in the formation pattern of the secondary zone with the vortices. In the separation flow past a rib, larger vortex structures emerge in the mixing layer compared to the case of the downward step. These structures, hitting the surface, form a flow-reattachment region whose time-mean boundary, in contrast to the case of a downward step, seems not to be in contact with the sidewalls, which provides indirect evidence for large dimensions of these vortex formations. Behind the rib, intense vortices whose scale is quite comparable with the obstacle height are observed in the corner zone. At the same time, such vortices behind the downward step are seen indistinctly, with a mushroom-like structure emerging in the central part of the secondary zone. Thus, the secondary zone

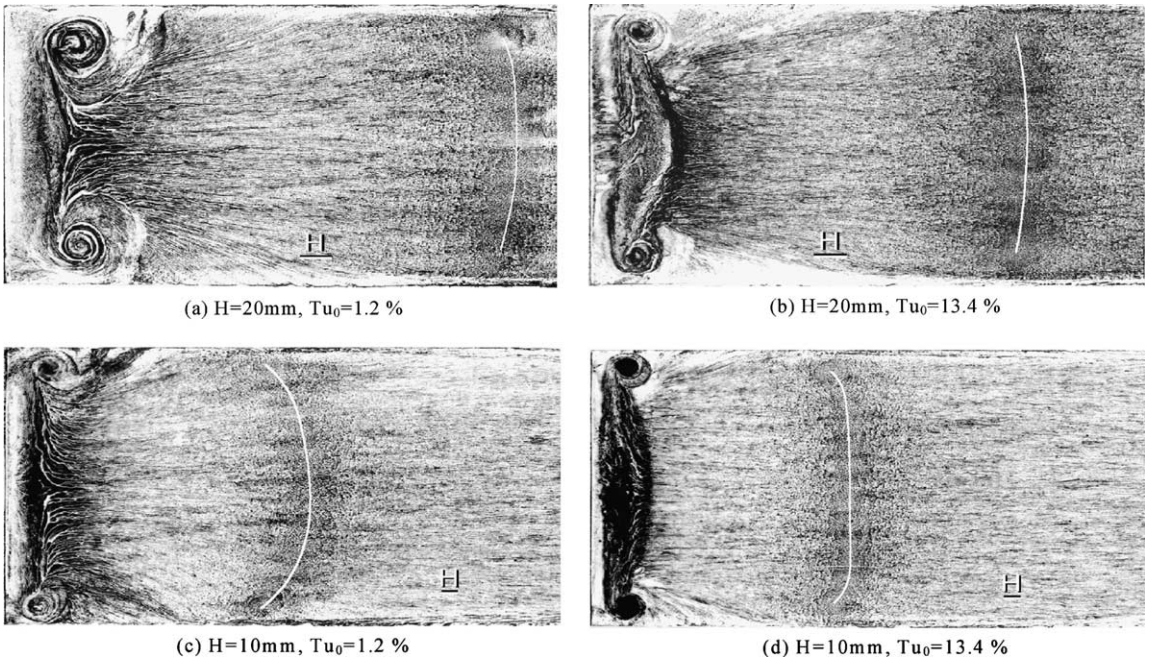

Fig. 7. Comparison of the surface flow patterns behind rib of height 20 mm (a; b) and 10 mm (c; d) at a low level free-stream turbulence (a; c) and in high-turbulized flow (b; d). Look from above. Direction of the free-stream from the left to the right. Figs. 7 and 8 were carried out on a identical scale.

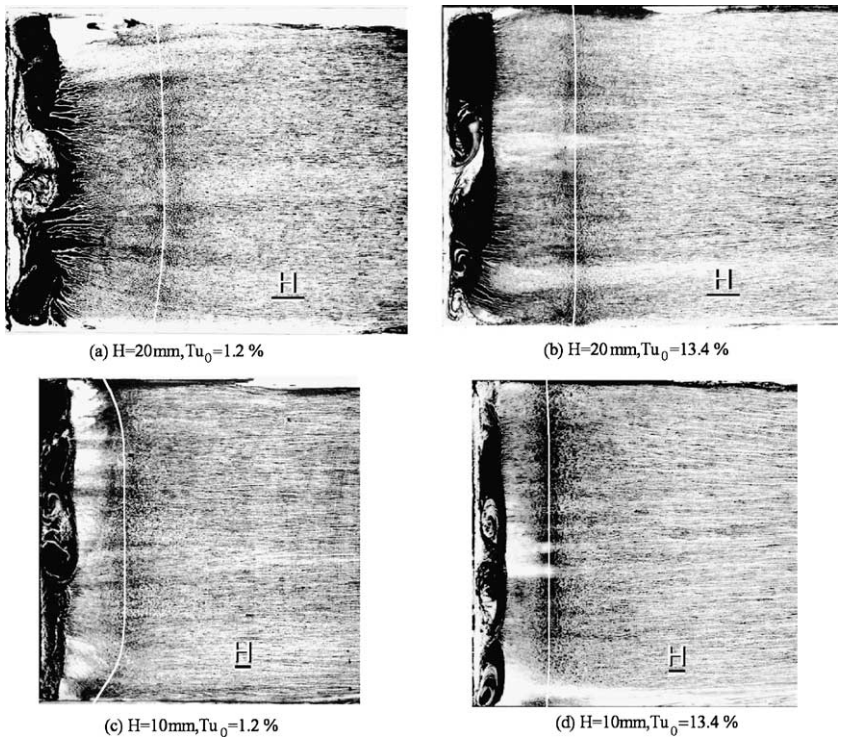

Fig. 8. Comparison of the surface flow patterns behind step of height 20 mm (a; b) and 10 mm (c; d) at a low level free-stream level (a; c) and in high-turbulized flow (b; d). Look from above. Direction of the free-stream from the left to the right.

represents a characteristic feature of the separation flows past a rib and past a step; this zone behind the rib is symmetric and more intense than behind the step, and its length is greater.

Behind the rib of height $H = 20$ mm under conditions of natural turbulence of the main flow (Fig. 8a), the near-surface flow is rather symmetric. The time-mean reattachment point of the separated flow on the symmetry axis of the model lies at $x_R/H = 4.8$, with a typical amplitude of oscillations in the streamwise direction equal to about half the step height, which is somewhat smaller than the oscillation amplitude of the flow-reattachment point behind the rib. The transverse size of the secondary vortex changes from about 20% of the total length of the separation bubble near the walls to about 40% of this length at the center. Under the same external conditions, the time-mean reattachment curve of the flow behind the 10-mm step (see Fig. 8c) is more bent, being separated from it along the centerline by the distance $x_R/H = 5.5$.

Under conditions of highly turbulized incoming flow, the secondary region behind the downward step is asymmetric, while the reattachment curve is more rectified, providing an indication for reestablishment of two-dimensionality in the turbulent flow. In the case of the high-turbulence flow, the recirculation zone becomes shorter by 0.8 of caliber behind the downward steps of either height (see Fig. 8b and d). The shrinkage of the recirculation-flow region can be explained by widening of the mixing layer predominantly in the downward direction, due to which a rapider reattachment of the separated flow takes place. Under these conditions, the secondary vortex displays asymmetry not only at the center near the step but also near the sidewall, where the main vortex can disintegrate into two smaller vortices. Thus, our observations contradict the conclusion, made in [15], that an increase in the free-stream turbulence level causes no appreciable changes in the structure and length of the main and secondary recirculation-zone vortices; they show that high turbulence of the outside flow results in deformation of the separation bubble and causes notable changes in the structure of the secondary-vortex region.

Visualization data show that the increase in the free-stream turbulence results in shrinkage of the separation zone behind the 10- and 20-mm ribs by 3.5 calibers, whereas the analogous shrinkage of the separation zone behind the downward step amounts only to 0.8 of caliber, the relative shrinkage in this case being even smaller. The high level of free-stream turbulence causes no structural deformation of the secondary-vortex region behind the rib, but exerts a profound influence on the flow behind the downward step. This effect seems to be due to the difference in the pre-history of the flow approaching the obstacle. In the upstream region of a rib, there emerges an additional separated flow that blocks the effect due to enhanced free-stream turbulence.

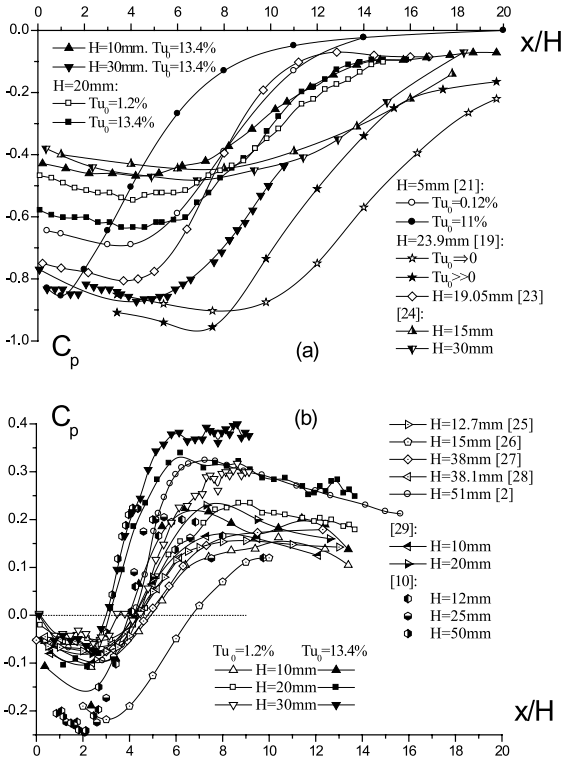

Fig. 9. Pressure coefficients behind a rib (a) and a step (b).

The data on the distributions of static pressure behind the obstacles make it possible to gain a better insight into the structure of the separation flow as a whole, this structure determining the friction and heat transfer. The behavior of static pressure behind obstacles of various heights (see Fig. 9, which shows the static-pressure data given in the form of the pressure coefficient $C_p = 2 \cdot (P_i - P_0)/\rho U_0^2$, where P_i is the static pressure in the flow separation region, and P_0 and U_0 are the free-stream pressure and free-stream flow velocity) agrees well with previously reported data [10,21–29]. The entire flow region behind the rib (see Fig. 9a) is occupied by a rarefaction zone, and the pressure difference vanishes only in the immediate vicinity of the flow-reattachment point. Some local decrease of $|C_p|$ over initial calibers up to the point where this coefficient attains its maximum confirms the occurrence of the secondary vortex. Behind the downward step (see Fig. 9b), the surface static pressure first somewhat decreases in the downstream direction and then abruptly increases, providing an indication for the fact that the flow indeed reattaches the surface. Here, the reattachment of the flow occurs prior to the point where the pressure coefficient attains its highest. It should be noted that, in spite of the substantial scatter of the experimental data, there is qualitative similarity between the static-pressure

distributions over the model surface, both behind ribs and steps.

The enhanced free-stream turbulence increases rarefaction in the recirculation region behind obstacles (Fig. 9) and exerts a profound effect on the flow in the flow-reattachment region. The maximum pressure difference caused by the intense artificial turbulization of the main flow is observed in the vicinity of the point where the low-turbulence flow over the obstacle attaches the surface. The enhanced external turbulence exerts a stronger action on the shift of the C_p maximum towards the obstacle than on the shift of the flow-reattachment region. In the relaxation region, the effect of enhanced external turbulence on C_p becomes weaker and displays saturation. This result can be attributed to the fact that turbulization of the free flow affects this region only via the normal component of pulsating velocity.

A comparison between the distributions of the normalized pressure coefficient $\overline{C}_p = (C_p - C_{p\min})/(1 - C_{p\min})$ [30] behind the obstacles shows that these distributions behind ribs (Fig. 10a) are automodel with respect to the rib height and level of free-stream turbulence. Note that previously reported studies give no examples of successful generalization of experimental static-pressure data for the flow past a rib under different flow conditions and turbulence levels. Some scatter of the experimental data is observed only in the downstream region of the flow-reattachment point. At the same time, we failed to obtain satisfactory generalization of static-pressure data in the same relative coordinates for steps of various heights, including data previously reported by other workers. We believe that this fact can be attributed to the effect of flow pre-history (and, in particular, relative thickness of the boundary-layer upstream of the step) on flow separation (see Fig. 10b). For the artificially turbulized flow, the situation somewhat improves.

Consider now the behavior of the maximum velocity of the reverse flow, which determines the boundary of the new boundary layer developing in the direction from the flow-reattachment point towards the obstacle. These data are necessary for generalization of heat-transfer data, and also for developing adequate prediction algorithms for friction and heat and mass transfer in the recirculation region. The maximum velocity of the reverse flow in the recirculation region behind the 20-mm rib amounts to 40% of the free-stream velocity (Fig. 11). The distribution of the maximum velocity displays the following characteristic features. First, the flow accelerates from the flow-reattachment point, and then it decelerates up to the point where its secondary detachment from the wall occurs. The experiments reveal some decrease of the maximum velocity with decreasing obstacle height. This decrease can be attributed to the increase of the velocity gradient on the flow spreading line. A decrease in the obstacle height to 10 mm results in an insignificant decrease of the maximum velocity of the reverse flow and shifts the position of the maximum closer to the rib. The maximum velocity of the reverse flow behind the downward step is substantially lower than behind the rib. For instance, this velocity behind

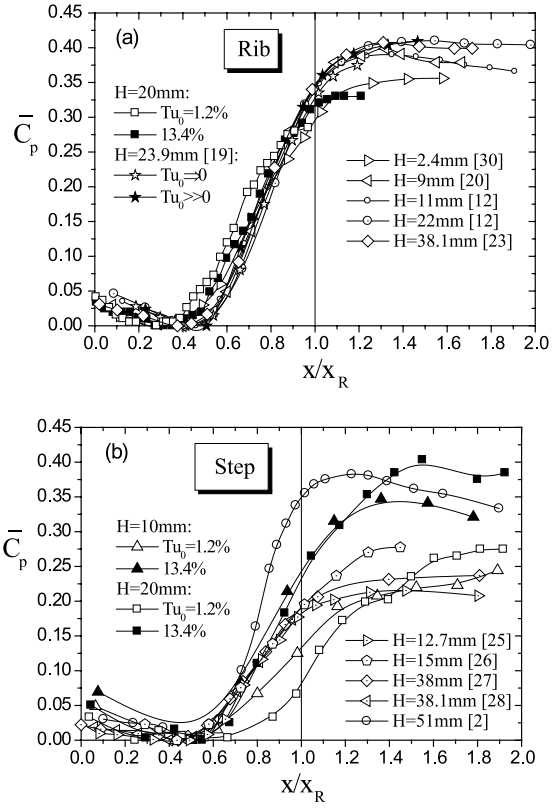

Fig. 10. Reduced pressure coefficients behind a rib (a) and a step (b).

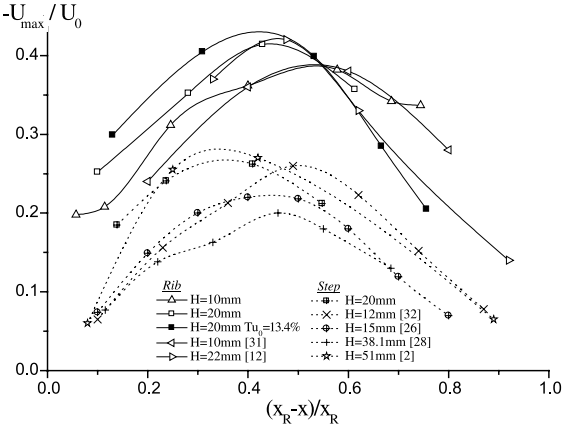

Fig. 11. Maximum velocity of the reverse flow in the recirculation region [2,12,26,28,31,32].

the 20-mm high step equals about 25% of U_0. These data well agree with the data obtained in other studies (see Fig. 11).

Enhanced external turbulence accelerates the recirculation flow both behind ribs and behind steps. This conclusion agrees with the data for a downward step obtained in [17], in which a 10–15% increase in the maximum recirculation velocity was reported. On the whole, as it can be concluded from Fig. 11, in spite of the substantial differences in the experimental conditions used in different studies, there is quite a good correlation between the experimental data, both for ribs and for steps; this correlation can be used in engineering analysis.

A separation region behind a single obstacle itself is a source of intense turbulence. The maximum intensity of this turbulence near the obstacle is observed in the middle part of the mixing layer, and this turbulence further increases in the downstream direction. Fig. 12 shows the position of the maximum root-mean-square pulsations of flow velocity behind a rib and behind a step. The smaller the recirculation flow region in the relative form, the closer to the surface the turbulence maximum lies. Under natural external conditions, strong turbulization is observed behind a low-height rib ($H = 6$ mm) even at distances exceeding $y/H = 2$ [34]. Under the presence of a high free-stream turbulence ($Tu_0 = 13.4\%$), its notable influence on the distribution of turbulent flow pulsations is observed in the region as high as three calibers and even behind the flow-reattachment region (Fig. 12), in line with the data obtained in [19]. The maximum turbulence level that develops in the mixing layer moves from the obstacle and from the surface, and, approaching the model, attains its absolute maximum approximately at the point with the coordinates $x/H = 13.3$ and $y/H = 2$ for the 6-mm high rib and at the point with the coordinates $x/H \approx 4.4$–6.1 and $y/H \approx 0.5$ for the 20-mm high downward step; it further

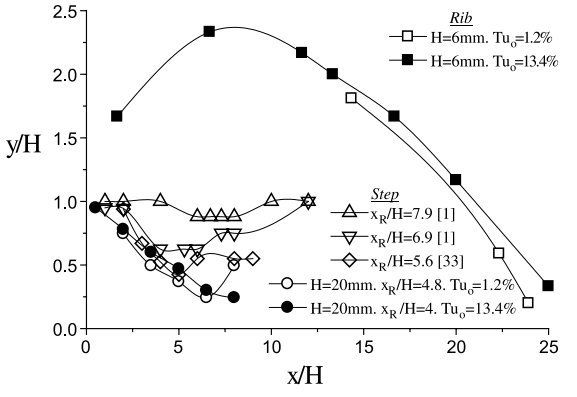

Fig. 12. Maximum turbulence intensity distribution behind a rib and a step [1,33].

decreases while approaching the plate. The fact that the absolute turbulence maximum is situated in the vicinity of the flow-reattachment point or somewhat upstream of it was reported previously in [11,17] and in [1] (1–2 calibers) and [5,35] (1.5 calibers), respectively. This can be explained by the fact that, first, the streamline that attaches the surface at the flow-reattachment point belongs to the newly developing viscous layer and, second, the reverse flow at the flow separation point increases the effective difference between the flow velocities across the new viscous layer in this region, thus increasing the level of turbulent pulsations.

Note that, as the level of free-stream turbulence increases, the maximum of velocity pulsations moves closer to the obstacle, providing further evidence for shrinkage of the reverse-flow region. In this situation, the enhanced free-stream turbulence results in some expansion of the mixing layer, due to which internal fluctuations are transferred to the outside boundary, and in a rapider growth of the low-velocity slope compared to the case of natural-turbulence conditions.

3.2. Heat transfer. Impact of enhanced free-stream turbulence

Consider the downstream evolution of the heat-transfer coefficient along the symmetry plane of the plate. Fig. 13 shows the distribution of this coefficient behind ribs (a, c) and behind downward steps (b, d) of various heights for the cases of low- (a, b) and high-turbulence (c, d) flow. The heat-transfer coefficient was found from the difference between the wall temperature and the flow core temperature: $\alpha = q_w/(T_w - T_0)$. For comparison, the same figure shows the experimental data obtained at identical Reynolds numbers for the flow without separation (on a smooth plate without an obstacle). Note the characteristic features of shown data. A decrease in the obstacle height results in a considerable increase of the heat-transfer maximum. The maximum is situated closer to the obstacle. For the flow with separation past a rib, the heat-transfer maximum is shifted farther in the downstream direction from the flow separation point compared to the case of a downward step. The flow past a rib (Fig. 13a) displays no rapid boundary-layer recovery in the relaxation zone, in the downstream region of the flow-reattachment point, because of the thick mixing layer that forms in this case. In the flow past a downward step (Fig. 13b), the heat-transfer coefficient in the relaxation zone approaches the values typical of the smooth plate more rapidly. In spite of the substantial difference between the structure of the flow past a rib and the structure of the flow past a step, and different rarefactions in the recirculation regions of the two flows, the maximum level of the heat-transfer coefficient behind the rib is only slightly lower than that behind the step.

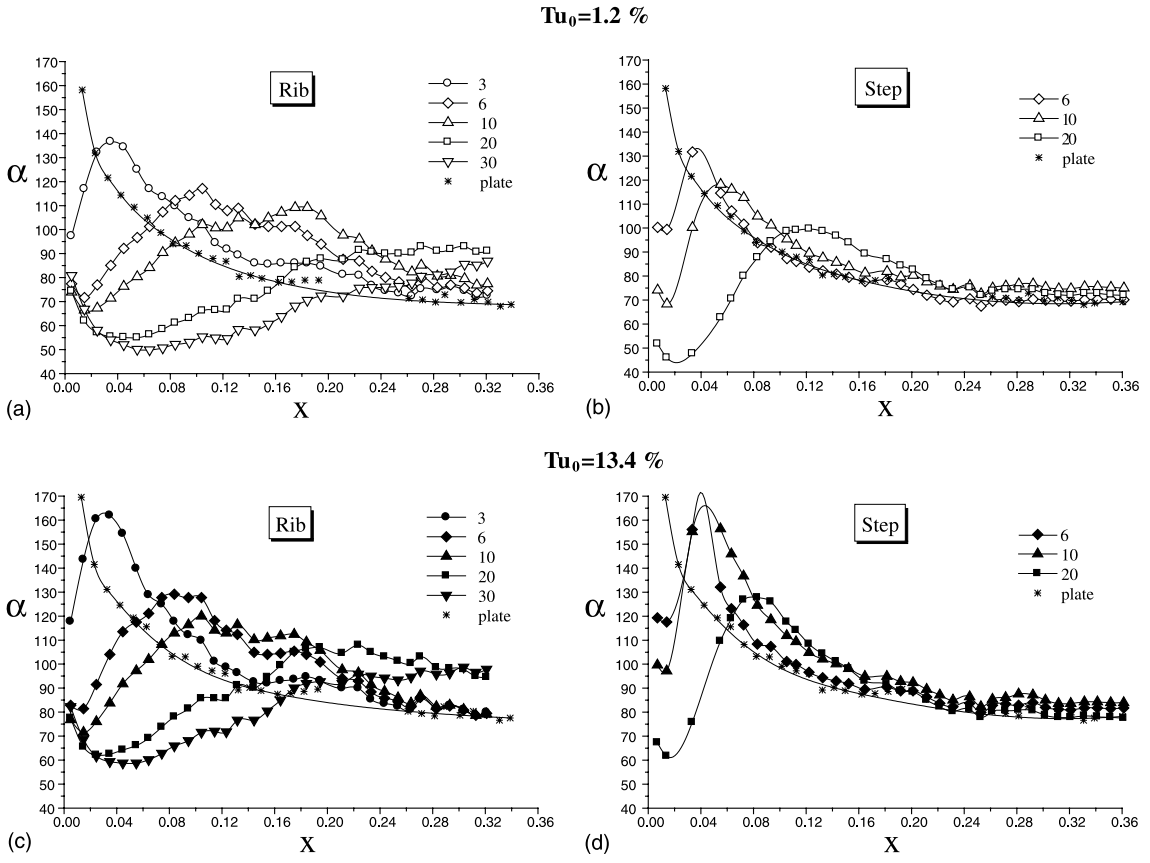

Fig. 13. Heat-transfer coefficient [W/(m^2 K)] distribution along the symmetry plane behind rib of height 3, 6, 10, 20, and 30 mm (a, c) and behind step of height 6, 10, and 20 mm (b, d), also on a plate in identical conditions at different free-stream turbulence levels.

Artificial turbulization of the free flow enhances the rate of heat transfer behind the obstacles and leads to displacement of the heat-transfer maximum in the upstream direction. Behind ribs (Fig. 13c), the maximum increase in the rate of heat transfer under the action of heavily turbulized flow is observed at a height of 3 mm; this increase amounts to about 15% of the value of α_{max} for the low-turbulence flow regime. The increase in α_{max} behind steps is more pronounced (Fig. 13d), amounting to $\alpha_{max\,Tu_0=13.4\%}/\alpha_{max\,Tu_0=1.2\%} \approx 1.3$ for the 20-mm high step. With decreasing step height, the intensification degree increases for a step with $H = 10$ mm, the observed increase in the heat-transfer coefficient is already about 40%.

Consider the effect of free-stream turbulence level on the heat transfer behind the obstacles. Fig. 14 illustrates the effect of enhanced free-stream turbulence on the local rate of heat transfer behind ribs (a) and downward steps (b) of various heights. An increase in the free-stream turbulence to $Tu_0 = 5\%$ weakly intensifies heat transfer. The maximum heat-transfer intensification behind a rib (see Fig. 14a), although manifested over a considerable length, amounts to only about 10%. For a downward step with $H = 30$ mm, a 20% heat transfer intensification, although over a twice shorter length, is observed. An increase in the turbulence level of the free-stream flow to 13.4% substantially enhances heat transfer behind the obstacles, the effect being more pronounced for steps. The maximum increase in the rate of heat transfer behind ribs (Fig. 14a) is about 35% ($H = 30$ mm). The largest heat-transfer intensification is observed for high ribs. This can be explained by the fact that, as the rib height decreases, the turbulence level near the leading edge of the rib increases even without artificial turbulization of the free flow; in fact, the flow separates from the surface under conditions with even higher turbulence. The highest intensification behind a downward step (Fig. 14b), observed for $H = 20$ mm, amounts to 75%. The following tendency can be traced in the flow-relaxation region: the smaller the obstacle height, the more pronounced intensification of heat transfer, induced by enhanced external turbulence, is observed. Thus, in spite of the fact that enhanced turbulence has a considerable intensifying effect on the rate

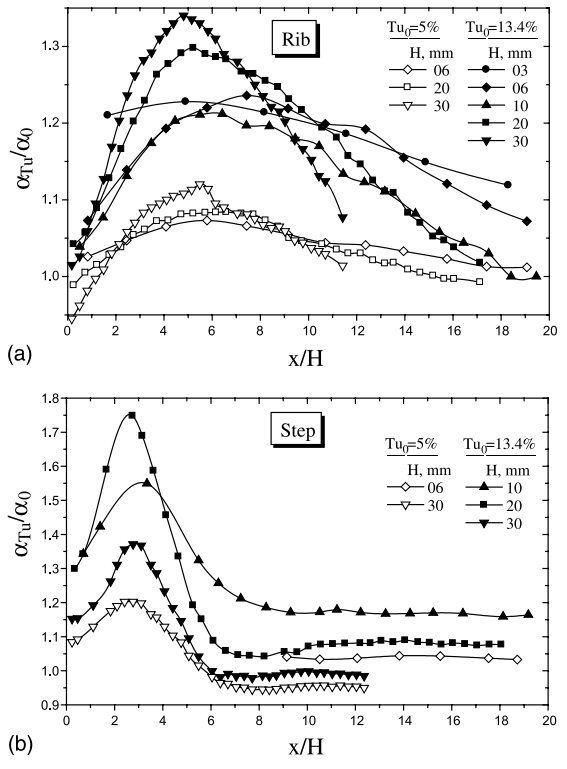

Fig. 14. Effect of enhanced external flow turbulence on local normalized heat-transfer coefficient distribution behind rib behind rib (a) and step (b) of various height. α_0 for $Tu_0 = 1.2\%$.

of heat transfer behind high obstacles, whatever the level of external turbulence, low obstacles offer more advantages as heat-transfer intensifiers (Fig. 13).

Consider the heat-transfer processes in the separation flows behind the obstacles. Fig. 15 depicts typical distributions of temperature behind the 20-mm high rib (a, b) and behind the 20-mm high downward step (c, d) observed at two levels of free-stream turbulence. It is seen from the profiles of dimensionless temperature that the highest thermal resistance takes place near the wall, especially in the case of the flow past the step. In the corner zone, where the mixing of the flows is weak because the rotation velocity of the vortex structure is low, the thermal head is maximal, both in the thin near-wall region and outside it. Under natural external turbulence, the local temperature behind the rib at the height $y/H = 3$ levels out at a temperature close to the free-flow temperature (Fig. 15a). The relative temperature in the region occupied by the main-recirculation vortex suffers drastic changes because of longitudinal transfer of heat by the reverse flow away from the surface. All profiles display an inflection point observed upstream of the flow-reattachment point. The profiles gradually level out in the downstream direction. Behind the downward step, the interaction between the main flow and the separation-flow temperature field proceeds below the level $y/H = 1$ (Fig. 15c). The core of the recirculation flow displays a strong deformation of the temperature profiles, whereas no such deformation is observed behind the rib. The temperature profiles in the secondary zone approach the main-stream temperature approximately at the same distance from the wall as the profiles for the recirculation and relaxation regions do, whereas the profiles behind the rib approach this temperature much earlier. In the near-wall zone behind the step, and also in the mixing layer, considerable temperature changes are observed, in line with the findings of [11,36].

With increasing free-stream turbulence level, the rate of heat transfer in the separation region increases, the wall temperature substantially diminishes, and the thermal-mixing layer becomes wider. At the initial stage (over the length occupied by the secondary vortex), these changes occur due to the widening of the upper boundary (Fig. 15b). This tendency is retained over the whole main-recirculation region behind the higher rib, while the thermal-mixing layer behind the smaller rib ($H = 10$ mm) develops at the expense of the lower boundary. As a result, the dimensionless temperature in the core of the main-recirculation flow decreases behind the 20-mm rib and increases behind the 10-mm rib under the action of the high-turbulent incoming flow. In the downstream region of the rib, the high-turbulence external flow (Fig. 15d) gives rise to substantial changes of the thermal-mixing structure of the separation flow. Nevertheless, the corner zone remains rather conservative.

To represent the temperature profiles in universal coordinates, we used the thermal analogue of friction velocity in the form $\phi = \frac{T-T_w}{T_0-T_w} \cdot \frac{1}{\sqrt{St}}$; $\eta = yU_0 \frac{\sqrt{St}}{\nu}$.

Fig. 16 shows evolution of the temperature profiles. In this figure, curves 1 and 2 show the temperature profiles in the laminar sublayer and in the turbulent core of the classical boundary layer: $\phi = \eta$; $\phi = 5.5 + 2.5 \cdot \ln \eta$.

As it follows from the figure, the measured velocity profiles substantially differ from the standard distribution. This difference can be attributed to the fact that the major part of the logarithmic zone in the separation flow falls into the mixing and recirculation regions, where heat-transfer regularities substantially differ from the regularities typical for the near-wall turbulent flow. Simultaneously, all temperature profiles for the separation flow at both turbulence levels display a characteristic logarithmic part with an almost constant slope both in the recirculation and in the relaxation zone; this slope substantially differs from that displayed by the standard distribution (2). In the vicinity of the flow-reattachment region, the temperature profiles are automodel at both turbulence levels. This property seems to be of great significance as it can be used in developing models for turbulent heat transfer in separation flows.

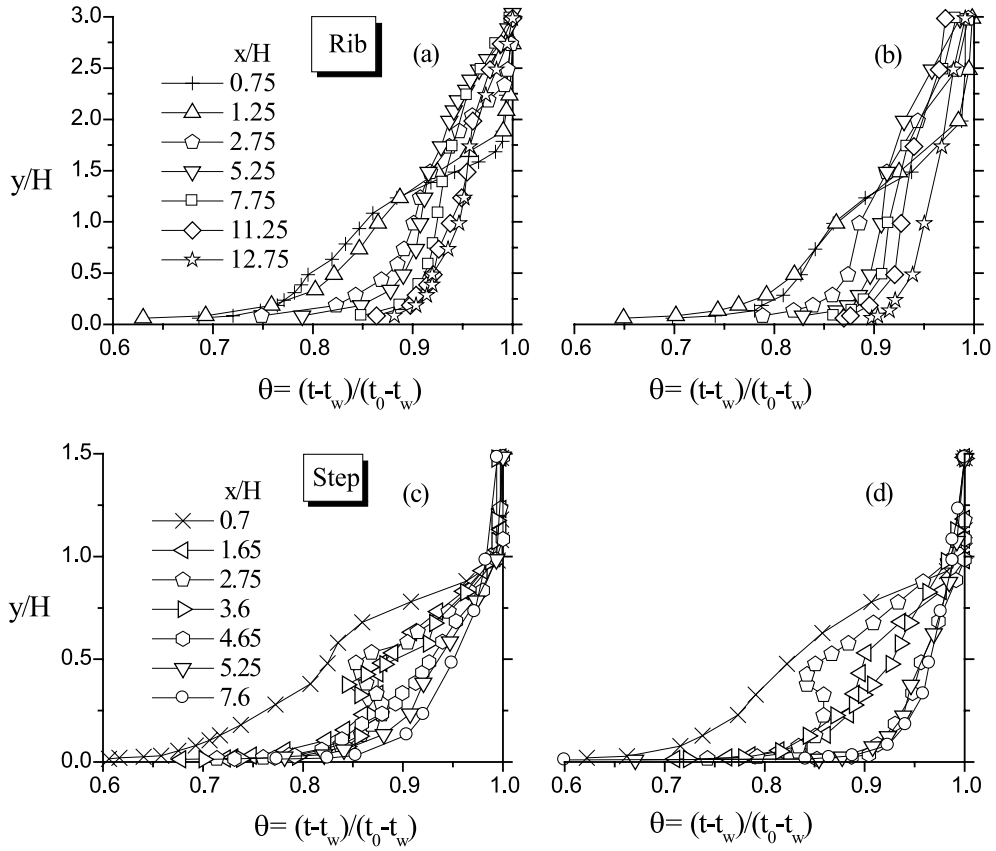

Fig. 15. Dimensionless temperature profiles behind a rib (a; b) and a step (c; d) at $Tu_0 = 1.2\%$ (a; c) and 13.4% (b; d).

Consider now convective heat-transfer regularities in the near-wall region, separately in the upstream and downstream regions of the flow-reattachment point. This approach makes it possible to analyze the development of the flow from the spreading point invoking the boundary-layer theory. The left- and right-hand sides of the graph in Fig. 17 refer to the recirculation and relaxation regions. The same graph shows data by other authors together with theoretically predicted curves for heat transfer in the standard laminar and turbulent boundary layers. In spite of the considerable scatter of experimental points, all experimental data for the relaxation region fall onto dependences with a slope typical of the turbulent flow mode ($m = 0.8$). This is observed both for ribs and for steps. The majority of experimental data obey the heat-transfer law for the standard turbulent non-separated flow within 20%. In the recirculation region, the picture is rather ambiguous. The experimental points for the initial development stage of the thermal boundary layer satisfactorily coincide (by the slope of the curve) with the dependence for turbulent heat transfer. Closer to the obstacle, the curve substantially deviates from the dependence $Nu_x = 0.036Re_x^{0.8}Pr^{0.4}$ because of the separation of the flow from the surface and the occurrence of a complex vortex flow in this region. On the whole, it is difficult to give a reasonable interpretation of the law of heat transfer in the recirculation region. Strictly speaking, an analysis based on using free-flow parameters is not perfectly adequate for the vortex reverse flow in the recirculation zone. In this region, under the complex conditions, a new boundary layer, similar to a near-wall submerged jet flow, develops, starting from the flow-reattachment point.

The experimental data for the recirculation region up to the secondary zone were also calculated from the parameters at the boundary of the near-wall region, where the reverse-flow velocity attains its highest. A similar representation of experimental data was used in [37] for the thermal problem and in [28] for the dynamic one. The data in this representation are shown in Fig. 18. The Reynolds number was calculated from the maximum velocity of the reverse near-wall flow: $Re_{xm} = U_{max} \cdot x^*/\nu$, where the coordinate x^* is reckoned from x_R in the upstream direction. The heat-transfer coefficient in the Nusselt criterion $Nu_{xm} = \alpha_m \cdot x^*/\lambda$ was

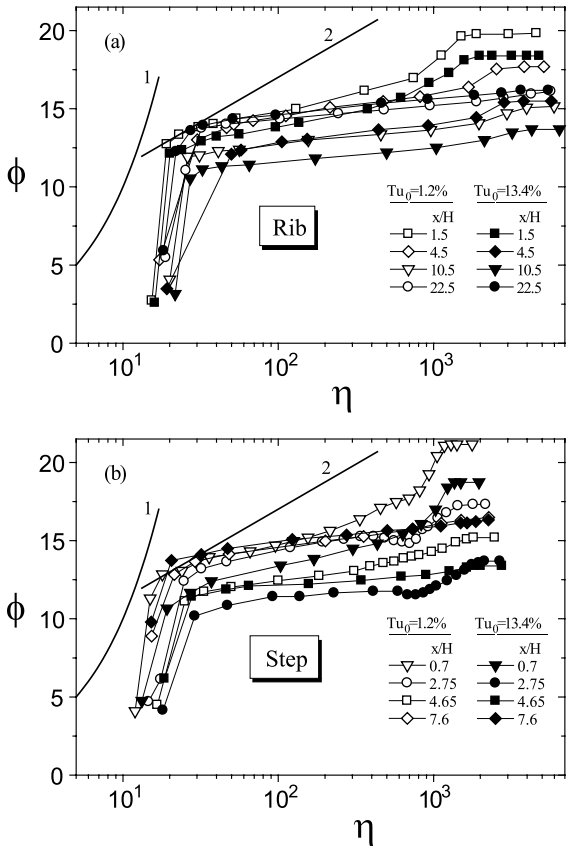

Fig. 16. Temperature profiles in universal coordinates: (a) behind rib ($H = 10$ mm) and (b) behind step ($H = 20$ mm). $Tu_0 = 1.2\%$ and 13.4%.

calculated from the difference between the wall temperature and the temperature at the position of the flow-velocity maximum: $\alpha_m = q_w(T_w - T_m)$. As is seen from Fig. 18, the experimental curves do not coincide with the laminar nor with the turbulent dependence for the flow over plate, although their slope more likely points to the turbulent law of heat transfer. This conclusion contradicts to the data of [28], in which surface friction was found to show a good agreement with the dependence for the laminar flow regime. According to the opinion expressed in [28], a main reason for flow laminarization is the strong action of the stabilizing longitudinal acceleration of the flow. Our estimates show that the acceleration parameter under the conditions adopted in the present study was well in excess of its critical value; however, no flow laminarization was observed in our experiments. All this shows that the approach used here to analyze the reverse flow under low- and high-turbulence conditions has only limited utility, being satisfactory only for the region occupied by the secondary corner flow.

3.3. Control of heat transfer in separation flows

As shown above, the separation flow is sensitive to variations of obstacle height and also to the action of heavily turbulized external flow.

Consider the joint effect due to obstacle geometry, varied by changing the inclination angle of the step face and the step height, and due to high free-stream turbulence. We consider separately the flows with and without separation over an inclined step and the effect of the

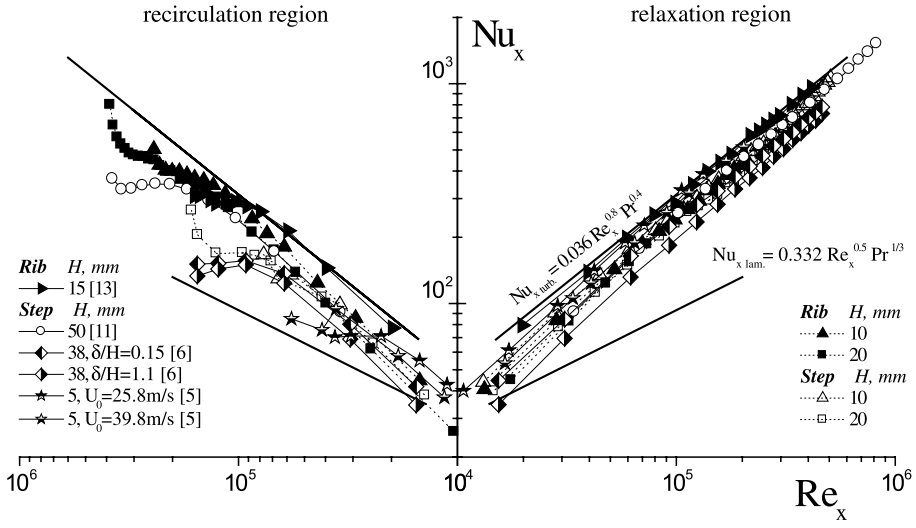

Fig. 17. Nusselt number calculated from the parameters of free stream behind obstacles in recirculation and relaxation regions. $Tu_0 = 1.2\%$.

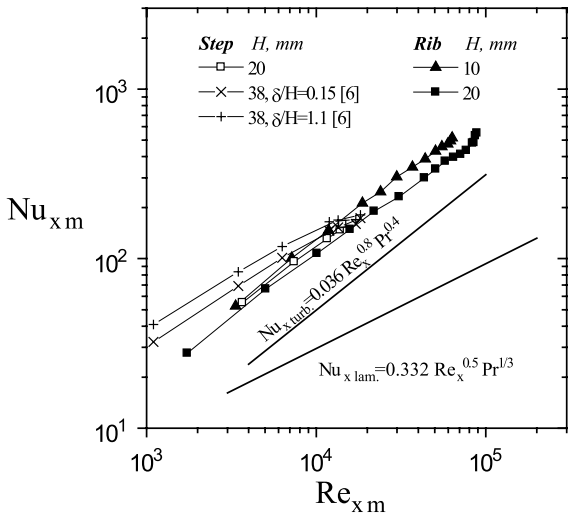

Fig. 18. Nusselt number calculated from the parameters of near-wall flow behind obstacles in recirculation region.

flow modes on the distribution of the heat-transfer coefficient. Without an external turbulence generator, a decrease in the step-face inclination angle β from 90° to 20° for the 20-mm high downward step intensifies heat transfer (Fig. 19a) and shifts the heat-transfer maximum in the upstream direction; this observation is consistent with the data of [11]. Here, the difference between the heat-transfer maxima is small, not exceeding 20%. The general heat-transfer level for $\beta = 15°$ is low since the flow in this case is non-separated. A rise in the level of free-stream turbulence results in an increase of the heat-transfer coefficient (Fig. 19b). For the 20-mm high step with $\beta = 45°$, the heat-transfer maximum increases by ~30%. For $\beta = 20°$, the increase in α_{max} for $Tu_0 =$ 13.4% is the smallest one (lesser than 5%). The latter shows that the high-turbulence flow suppresses flow separation and tends to transform the flow with separation into the flow without separation.

Under natural-turbulence conditions, the flow behind the 10-mm high inclined step with $\beta = 15°$ displays no separation [38], as well as the flow for $H = 20$ mm, and the observed heat-transfer pattern for $\beta = 20°$, which shows an abrupt decrease in the rate of heat transfer, closely resembles that for the flow without separation. A maximum rate of heat transfer for $H = 10$ mm was observed behind an inclined step with $\beta = 30°$. Unlike the cases of 20- and 50-mm high steps [11], this maximum is gently sloping and less pronounced (see Fig. 20). The heat-transfer maximum for the step with $H = 10$ mm and $\beta = 20°$ has a lowest amplitude among all maxima displayed by separation flows over the steps, being close to that for the flow without separation. The same regularity was displayed by the step with $H = 20$ mm streamlined by the flow with $Tu_0 = 13.4\%$. A comparison between the distributions of the heat-transfer

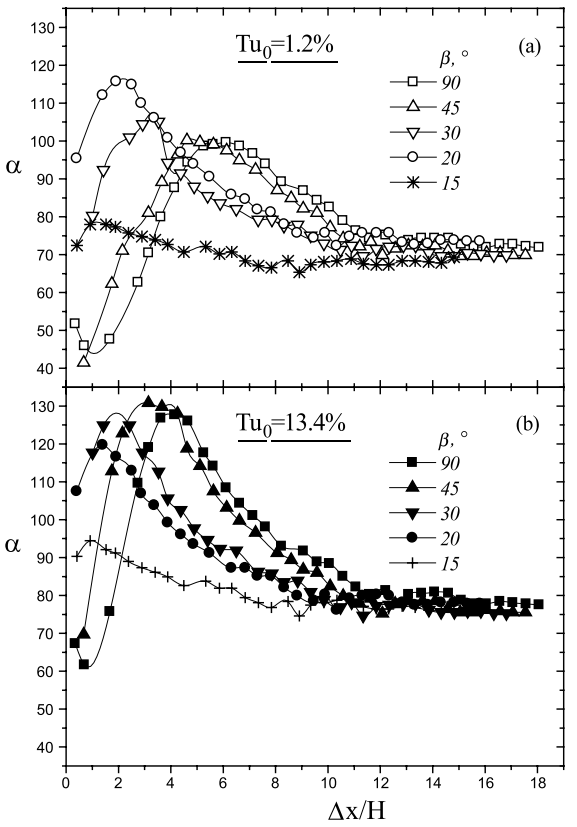

Fig. 19. Heat-transfer coefficient [W/(m^2 K)] behind an inclined step. $H = 20$ mm, $Tu_0 = 1.2\%$ (a) and 13.4% (b).

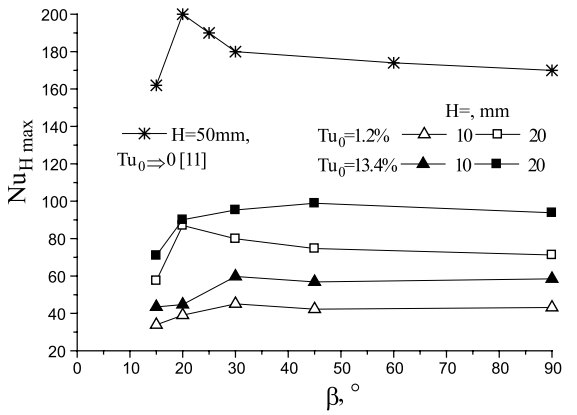

Fig. 20. Dependence of maximum Nusselt number upon the step angle at a different external turbulence level.

coefficient and between the heat-transfer maxima behind the inclined steps with $H = 10$ and 20 mm shows the coefficient α_{max} for the smaller step to be greater than that for the step with $H = 20$ mm in all cases except for $\beta = 20°$. The rate of heat transfer in the region occupied

by the secondary vortex behind the 10-mm high inclined step is greater than behind the 20-mm high step, whereas the rates of heat transfer in the flow-relaxation region are almost identical. The rate of heat transfer in the flow without separation ($\beta = 15°$) behind the step with $H = 10$ mm is 1.2 times greater than behind the step with $H = 20$ mm; the rates of heat transfer at the distance $\Delta x/H = 15$ are roughly identical. With increasing free-stream turbulence level, we also observed an increase in the rate of heat transfer behind the 10-mm high step. For the step with $\beta = 30°$, the heat-transfer coefficient increases by more than 30%. In the case of the 10-mm high step, the enhanced free-stream turbulence of the main flow leads to an earlier transition to the flow without separation (this transition is observed at $\beta = 20°$; see Fig. 20). It should be noted that the effect of heat-transfer intensification by high-turbulence outside flow in the relaxation region is only slightly greater in the case of flow without separation than in the case of step-face inclination angles giving rise to flows with separation.

The efficiency of an obstacle as a heat-transfer intensifier can be estimated from average characteristics, by comparing them with those for a flat plate. Fig. 21 shows the distribution of the mean heat-transfer coefficient behind a rib and behind a step, normalized to the analogous coefficient for a flat plate without an obstacle, obtained at two levels of free-stream turbulence. The data for ribs, both for natural external conditions (a) and for the heavily turbulized incoming flow (b), show low-height obstacles to be better heat-transfer intensifiers. Their maximum efficiency at low turbulence is about 15%, and it amounts to 20% under the conditions of enhanced free-stream turbulence. High ribs with $H > 10$ mm are ineffective heat-transfer intensifiers ($\bar{\alpha}_{rib}/\bar{\alpha}_{plate} < 1$). The action of high free-stream turbulence on heat transfer is insufficient for raising the efficiency of such ribs. Under natural-turbulence conditions, almost all

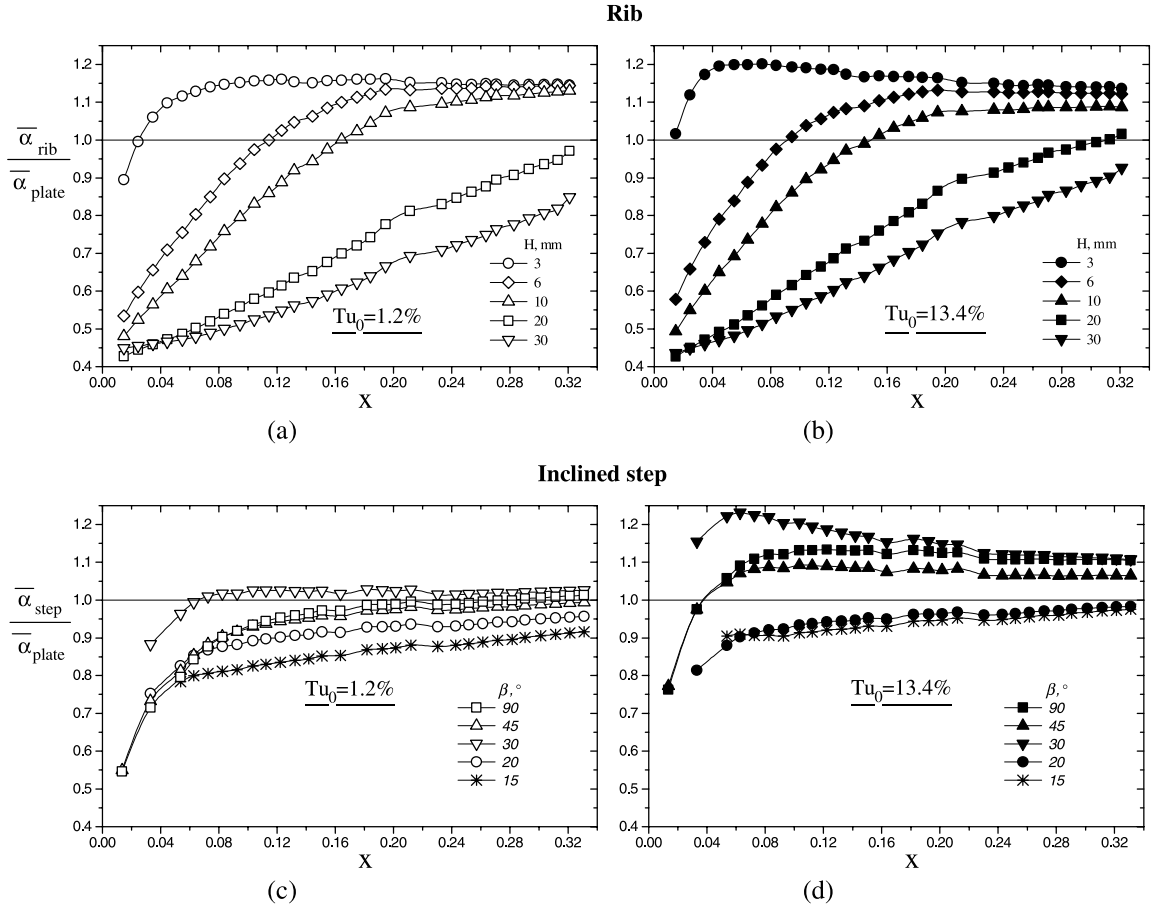

Fig. 21. The efficiency of a rib of a different height (a; b) and an inclined step of height 10 mm (c; d) as average heat-transfer intensifier at low (a; c) and high (b; d) free-stream turbulence level.

inclined steps of height 10 mm are also ineffective (see Fig. 21c). Almost throughout the entire explored length, a weak intensification effect (lesser than 5%) was observed only for $\beta = 30°$. Heavy artificial turbulization of the free flow substantially raises the efficiency of 10-mm high steps (d) for all inclination angles, giving rise to flows with separation. Inclined steps with no-separation angles remain ineffective heat-transfer intensifiers. Under high-turbulence conditions, the maximum relative thermal efficiency at all other conditions kept unchanged (about 25%) was observed behind the step with $\beta = 30°$ (Fig. 21d). The effect of high-turbulence incoming flow on thermal characteristics depends on the step-face inclination angle and on the step height, which fact emphasizes the importance of the inter-relation of the three parameters: step height, step-face inclination angle, and level of free-stream turbulence.

Thus, the recirculation-region length, the mixing-layer thickness, and the position of maximum values of pressure and heat-transfer coefficients all depend on the geometry of the separation flow. Changing parameters of the separation flow and the free-stream turbulence level, one can control the turbulent separation, either suppressing or intensifying heat transfer.

4. Summary

Enhanced external turbulence results in widening of the shear layer and, as a consequence, in almost identical (in the relative form) shrinkage of the separation region both for ribs and downward steps of various heights. In this case, rectification of the flow-reattachment curve in the transverse direction is observed. The study has revealed a distinct difference between the structures of secondary vortices generated in the separation flows past a rib and past a step both at low and high-turbulence levels.

It is found that the distribution of surface pressure behind the flow separation point can be generalized in universal coordinates for ribs of various heights and various levels of external turbulence. No such generalization was obtained for the flow past a downward step because of the substantial effect of flow pre-history on the flow structure.

A high-turbulence incoming flow appreciably intensifies the local heat-transfer rate behind the obstacles, the effect being more pronounced for the flows past steps. In both cases, the intensification of heat transfer in the relaxation zone is more pronounced for smaller heights of the obstacles.

The experimental data for heat-transfer upstream of the point where the rate of heat transfer is maximal to the secondary-vortex zone, treated using parameters at the internal boundary of the main vortex, obey the turbulent heat-transfer law.

Judging from local and average characteristics, smaller obstacles seem to be more promising heat-transfer intensifiers. In this respect, ribs are more effective than steps. On the other hand, the efficiency of steps as heat-transfer intensifiers can be raised by varying the degree of free-stream turbulence and the inclination angle of the step face. Enhanced free-stream turbulence suppresses flow separation and increases the angle at which the flow becomes non-separated.

Acknowledgements

This work was supported by the Russian Foundation for Fundamental Research (Grant Nos. 01-02-16842 and 03-02-06088-mas) and by the Russian-Federation Presidential Foundation for Leading Scientific Schools (Grant No. NSh-1308.2003.8).

References

[1] J.K. Eaton, J.P. Johnston, A review of research on subsonic turbulent flow reattachment, AIAA J. 19 (9) (1981) 1093–1100.
[2] C. Chandrsuda, P. Bradshaw, Turbulence structure of a reattaching mixing layer, J. Fluid Mech. 110 (1981) 171–194.
[3] D.W. Etheridge, P.H. Kemp, Measurements of turbulent flow downstream of a rearward-facing step, J. Fluid Mech. 86 (3) (1978) 545–566.
[4] P.P. Zemanick, R.S. Dougall, Local heat transfer downstream of abrupt circular channel expansion, J. Heat Transfer 92 (1970) 53–60.
[5] P.L. Komarov, A.F. Polyakov, Study of turbulence and heat-transfer characteristics behind a downward step in a slit channel, IVTAN Preprint No. 2-396, 1996, pp. 1–69 (in Russian).
[6] J.C. Vogel, J.K. Eaton, Combined heat transfer and fluid dynamic measurements downstream of a backward-facing step, Trans. ASME, J. Heat Transfer 107 (4) (1985) 922–929.
[7] A. Pedishius, A. Shlanchiauskas, Turbulent heat transfer in near-wall layers, Mokslas, Vilnius, 1987, pp. 1–239.
[8] T. Ota, H. Nishiyama, A correlation of maximum turbulent heat transfer coefficient in reattachment flow region, Int. J. Heat Mass Transfer 30 (6) (1987) 1193–1200.
[9] T. Ota, H.-G. Fu, H. Yoshikawa, Effects of aspect ratio on turbulent heat transfer around a downward facing step, in: Proceedings of Twelfth International Heat Transfer Conference, Grenoble, France, vol. 2, 2002, pp. 723–729.
[10] V.N. Kryukov, A study of turbulent separation behind a downward step, Collection of Topical Scientific Papers, Some Problems on Heat and Mass Transfer between Flows and Surfaces, 1986, pp. 24–28 (in Russian).
[11] T. Ota, Y. Sugawara, Turbulent heat transfer on the separated and reattached flow around an inclined downward step, in: Proceedings of Tenth International Heat

Transfer Conference, Brighton, UK, vol. 3, 1994, pp. 113–118.
[12] R. Ruderich, H.H. Fernholz, An experimental investigation of a turbulent shear flow with separation, reverse flow, and reattachment, J. Fluid Mech. 163 (1986) 283–322.
[13] E.P. Dyban, E.Ya. Epik, L.E. Yushina, Heat Transfer on the surface of longitudinally streamlined bodies in the presence of closed separation and external flow turbulization, in: Proceedings of Tenth International Heat Transfer Conference, Brighton, UK, vol. 3, 1994, pp. 25–30.
[14] R.L. Simpson, Turbulent boundary-layer separation, Ann. Rev. Fluid Mech. 21 (1989) 205–234.
[15] D.E. Abbott, S.J. Kline, Experimental investigation of subsonic turbulent flow over single and double backward-facing steps, Trans. ASME, J. Basic Engng. 84D (1962) 317–325.
[16] K. Isomoto, S. Honami, The effect of inlet turbulence intensity on the reattachment processes over a backward-facing step, Trans. JSME 54B (1988) 51–58.
[17] V.E. Alemasov, G.A. Glebov, A.P. Kozlov, Thermoanemometric Methods for Studying Flows with Separation, Kazan' Branch of the USSR Academy of Sciences, Kazan, 1989, pp. 1–178 (in Russian).
[18] G.H. Junkhan, G.K. Serovy, Effects of free-stream turbulence and pressure gradient on flat-plate boundary-layer velocity profiles and on heat transfer, Trans. ASME, J. Heat Transfer 89C (2) (1967) 58–68.
[19] I.P. Castro, A. Haque, The structure of a shear layer bounding a separation region. Part 2. Effects of free-stream turbulence, J. Fluid Mech. 192 (1988) 577–595.
[20] R. Hillier, N.J. Cherry, The effects of free-stream turbulence on separation bubbles, J. Wind Engng. Indust. Aero. 8 (1981) 49–58.
[21] Y. Nakamura, S. Ozono, The effects of turbulence on a separated and reattaching flow, J. Fluid Mech. 178 (1987) 477–490.
[22] I.P. Castro, A. Haque, The structure of a turbulent shear layer bounding a separation region, J. Fluid Mech. 179 (1987) 439–468.
[23] N.J. Cherry, R. Hillier, M.E.M.P. Latour, Unsteady measurements in a separated and reattaching flow, J. Fluid Mech. 144 (1984) 13–46.
[24] E.V. Vlasov, A.S. Ginevskii, R.K. Karavosov, M.O. Frankfurt, Near-wall pressure pulsations in the flow separation region behind two-dimensional obstacles, Trudy TsAGI, Iss. 2137 (1982) 3–29 (in Russian).
[25] D.M. Driver, H.L. Seegmiller, J. Marvin, Time-dependent behavior of a reattaching shear layer, AIAA J. 25 (7) (1987) 914–919.
[26] J.T. Yang, B.B. Tsai, G.L. Tsai, Separated-reattaching flow over a backstep with uniform normal mass bleed, Trans. ASME, J. Fluids Engng. 116 (1994) 29–35.
[27] S. Jovic, An experimental study of a separated/reattached flow behind a backward-facing step. $Re_H = 37,000$, NASA Technical Memorandum 110384, 1996.
[28] E.W. Adams, J.P. Johnston, Flow structure in the near-wall zone of turbulent separated flow, AIAA J. 26 (8) (1988) 932–939.
[29] I. Tani, M. Iuchi, H. Komoda, Experimental investigation of flow separation associated with a step or groove, Rept. 364, Aeronautical Research Institute, University of Tokyo, 1961.
[30] A. Roshko, J.C. Lau, Some observations on transition and reattachment of free shear layer in incompressible flow, in: Proceedings of the Heat Transfer and Fluid Mechanics, Stanford University Press, 1965, pp. 157–167.
[31] M. Kiya, K. Sasaki, Structure of a turbulent separation bubble, J. Fluid Mech. 137 (1983) 83–113.
[32] B. Makiola, B. Ruck, Experimental investigation of a single-sided backward-facing step flow with inclined step geometries, in: W. Rodi, E.N. Gani (Eds.), Engineering Turbulence Modelling and Experiments, Dubrovnik, Yugoslavia, 1990, pp. 487–496.
[33] S. Baker, Regions of Recirculating Flow Associated with Two-Dimensional Steps, PhD thesis, University of Surrey, Department of Civil Engineering, 1977.
[34] V.I. Terekhov, N.I. Yarygina, R.F. Zhdanov, The structure of the separated flow behind obstacles at high external turbulence, in: International Conference on the Methods of Aerophysical Research 9, Novosibirsk, Russia, vol. 1, 1998, pp. 220–227.
[35] T.-M. Liou, C.-F. Kao, Symmetric and asymmetric turbulent flows in a rectangular duct with a pair of ribs, Trans. ASME, J. Fluids Engng. 4 (1988) 373–379.
[36] E.V. Shishov, P.S. Roganov, S.I. Grabarnik, V.P. Zabolotsky, Heat transfer in the recirculating region formed by a backward-facing step, Int. J. Heat Mass Transfer 31 (1988) 1557–1562.
[37] A.I. Leontiev, V.I. Ivin, L.V. Grekhov, Semi-empirical method of the estimation of heat transfer in the region of boundary layer deattachment, J. Engng. Phys. 47 (4) (1984) 543–550.
[38] V.I. Terekhov, N.I. Yarygina, R.F. Zhdanov, Effect of free-stream turbulence on heat transfer behind a rib and inclined downward step, in: Proceedings of Eleventh IHTC, Korea, vol. 3, 1998, pp. 189–194.